ECCM-2001
European Conference on
Computational Mechanics
June 26-29, 2001
Cracow, Poland

Analysis of delamination growth with discontinuous finite elements

J.J.C. Remmers, G.N. Wells and R. de Borst
Koiter Institute Delft / Faculty of Aerospace Engineering
Delft University of Technology, Delft, The Netherlands
e–mail: J.J.C. Remmers@LR.TUDelft.nl

Key words: Delamination, composites, partition of unity, interfaces, debonding

Abstract. *Delamination is one of the most important failure mechanisms in laminates. Normally, it is modelled using interface elements. These elements are placed between two layers that are modelled with continuum elements. The interface elements are equipped with a softening or damage model in order to simulate debonding. This method has some drawbacks, both in a numerical and in a mechanical sense. A recent alternative is to simulate the crack by adding a discontinuous displacement mode to the continuum elements according to the partition of unity method. The elements do not contain the discontinuity prior to cracking, but when the ultimate stress in the bulk material is exceeded, delamination is initiated and additional degrees-of-freedom are activated. Beside this, a slightly different implementation is examined also. A discontinuity is predefined and has an initial dummy stiffness. Delamination is initiated when the tractions in the discontinuity exceed a threshold value. The results of both versions of this partition of unity model are compared mutually and with conventional interface elements by means of two examples.*

1 Introduction

One of the most important failure mechanisms in laminated materials is delamination, i.e. the debonding of two adjacent layers, caused by impact or stress concentrations at edges, holes or notches. In many cases, delamination occurs in combination with several other mechanical processes, such as matrix cracking and fibre splitting. Nevertheless, for reasons of simplicity, in numerical models, delamination is typically regarded as a single mechanism and is modelled with interface elements [1] which incorporate a nonlinear traction-separation relationship. A major disadvantage of this strategy is the fact that the path of the crack or delamination is predefined. This implies that the delamination front cannot develop into a matrix crack or a new delamination crack in a different interface. Furthermore, interface elements require an artificial 'dummy' stiffness, and tend to show spurious stress oscillations prior to cracking if the dummy stiffness is too high. As a remedy, lower dummy stiffnesses are often used in combination with alternative integration schemes [2].

An alternative to this approach is to insert discontinuities in continuum elements based on partitions of unity [3, 4]. The delamination crack is then represented by a discontinuity in the displacement field of the body [5, 6]. The magnitude of the displacement jump is governed by a number of additional degrees of freedom, which are added to each node whose support contains the discontinuity. An advantage of this method is that the additional degrees of freedom can be 'switched on' as a crack propagates. This means that prior to the initiation of the crack, the discontinuity is not present in the element, at variance with the interface model where high dummy stiffnesses must be used to simulate a perfect bond. The discontinuity is activated when the stresses at a specific material point of the bulk material exceed a threshold value. Debonding is then governed by a nonlinear traction-separation relationship at the discontinuity. Another benefit of the method is that since the trajectory of the crack is not predefined, deviation of the direction of crack growth and the interaction of two separate cracks can be simulated. Furthermore, the elements can also be used in unstructured meshes, whereas with the conventional method, the mesh must be built around the interface elements. Generally speaking, with this model, the mesh structure and the material structure are decoupled. This implies that the crack path is not captured by the shape and the density of the mesh and can arbitrarily progress through the model.

A simplified implementation can be considered also, in which the perfect bond of the discontinuity prior to delamination is simulated with a dummy stiffness. Debonding is initiated when the tractions in the discontinuity exceed a threshold value. Despite some of the benefits of the approach disappearing, it is still numerically more consistent than conventional interface elements, especially when geometrically nonlinearities are incorporated. Furthermore, the elements can still be used in unstructured meshes. In the remainder of this paper, we will refer to this element type as the *incorporated interface element*. In order to emphasise the distinction, the general formulation will be denoted as the *total enhanced element*.

This contribution is ordered as follows. In the next section, the kinematics of the continuum elements with an enhanced discontinuous mode are discussed. These relations are translated into a finite element description in section 3. The implementation of this description into a set

of geometrically linear four and eight-noded quadrilateral elements is explained in section 4. After that, the material (damage) model for the delamination is outlined. The performance of the new models is compared with that of conventional interface elements by means of two examples in section 6.

2 Kinematics

Consider a body Ω as shown in Figure 1. The body is divided into two parts, which will be denoted as Ω^- and Ω^+, on either side of the discontinuity Γ_d. The displacement field $\mathbf{u}(\mathbf{x},t)$ can be decomposed into two parts, a continuous and a discontinuous part, see also Wells *et al.* [5]:

$$\mathbf{u}(\mathbf{x},t) = \hat{\mathbf{u}}(\mathbf{x},t) + \mathscr{H}_{\Gamma_\mathrm{d}}(\mathbf{x})\,\tilde{\mathbf{u}}(\mathbf{x},t)\,, \tag{1}$$

where $\hat{\mathbf{u}}(\mathbf{x},t)$ and $\mathscr{H}_{\Gamma_\mathrm{d}}(\mathbf{x})\tilde{\mathbf{u}}(\mathbf{x},t)$ are the continuous and the discontinuous parts of the displacement field, respectively. $\mathscr{H}_{\Gamma_\mathrm{d}}(\mathbf{x})$ is the Heaviside function ($\mathscr{H}_{\Gamma_\mathrm{d}}(\mathbf{x}) = 1$ if $\mathbf{x} \in \Omega^+$ and $\mathscr{H}_{\Gamma_\mathrm{d}}(\mathbf{x}) = 0$ if $\mathbf{x} \in \Omega^-$). The strain field $\boldsymbol{\varepsilon}$ in the body can be calculated by taking the gradient of equation (1),

$$\boldsymbol{\varepsilon} = \nabla^s\hat{\mathbf{u}} + \mathscr{H}_{\Gamma_\mathrm{d}}\nabla^s\tilde{\mathbf{u}} + \delta_{\Gamma_\mathrm{d}}(\tilde{\mathbf{u}}\otimes\mathbf{n})^s\,, \tag{2}$$

where $\delta_{\Gamma_\mathrm{d}}$ is the Dirac-delta function centred at Γ_d and $\mathbf{n}$ is a normal vector to the discontinuity.

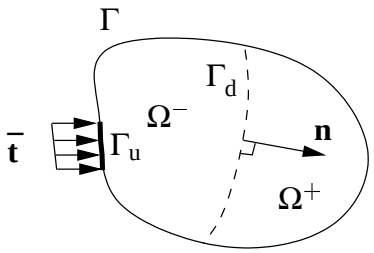

Figure 1: Domain Ω with a discontinuity Γ_d.

It is noted that all strains remain small, so the gradients correspond to the symmetric part only, which is denoted by $(\cdot)^s$. Equation (2) can be conceived as a summation of piece-wise continuous parts that govern the strains in the bulk material $\hat{\boldsymbol{\varepsilon}}$ and an unbounded part $\tilde{\boldsymbol{\varepsilon}}$ describing the strains at the discontinuity:

$$\hat{\boldsymbol{\varepsilon}} = \nabla^s\hat{\mathbf{u}} + \mathscr{H}_{\Gamma_\mathrm{d}}\nabla^s\tilde{\mathbf{u}}; \qquad \tilde{\boldsymbol{\varepsilon}} = \delta_{\Gamma_\mathrm{d}}(\tilde{\mathbf{u}}\otimes\mathbf{n})^s\,. \tag{3}$$

3 Finite element model

The displacement and strain fields from the previous section can be written in discrete format by using partitions of unity. Consider a collection of n functions $\phi_i(\mathbf{x})$, each belonging to a node

within the body Ω. These functions form a partition of unity if:

$$\sum_{i=1}^{n} \phi_i(\mathbf{x}) = 1\,. \tag{4}$$

It has been shown by Duarte and Oden [4] that a field can be interpolated in terms of discrete nodal values using partitions of unity. Using the function $\phi_i(\mathbf{x})$, an interpolation $u(\mathbf{x},t)$ over a body can be formed by:

$$u(\mathbf{x},t) = \sum_{i=1}^{n} \phi_i(\mathbf{x}) \left(a_i(t) + \sum_{j=1}^{m} b_{ij}(t)\gamma_j(\mathbf{x}) \right), \tag{5}$$

where ϕ_i are partition of unity functions, a_i are the regular nodal degrees of freedom, b_{ij} the additional nodal degrees of freedom and γ_j are enhanced basis terms.

Equation (5) can be transformed into finite element notation, since finite element shape functions form a partition of unity:

$$\mathbf{u}(\mathbf{x},t) = \mathbf{N}(\mathbf{x})\mathbf{a}(t) + \mathbf{N}(\mathbf{x})\left(\mathbf{N}_\gamma(\mathbf{x})\mathbf{b}(t)\right), \tag{6}$$

where $\mathbf{a}$ and $\mathbf{b}$ are vectors containing the regular and additional nodal degrees of freedom of the element, $\mathbf{N}$ is a matrix containing the shape functions and $\mathbf{N}_\gamma$ is a matrix containing the enhanced basis terms. To simulate the discontinuity, $\mathbf{N}_\gamma$ is replaced by a diagonal matrix containing Heaviside functions:

$$\mathbf{u} = \mathbf{N}\mathbf{a} + \mathscr{H}_{\Gamma_\mathrm{d}}\mathbf{N}\mathbf{b}\,. \tag{7}$$

The number of additional degrees of freedom per node is equal to the number of enhancements times the spatial dimensions. Differentiating equation (7) with respect to $\mathbf{x}$ and following the standard procedures [7] leads to:

$$\boldsymbol{\varepsilon} = \mathbf{B}\mathbf{a} + \mathscr{H}_{\Gamma_\mathrm{d}}\mathbf{B}\mathbf{b} + (\delta_{\Gamma_\mathrm{d}}\mathbf{R})\mathbf{N}\mathbf{b}\,, \tag{8}$$

where $\mathbf{B} = \mathbf{L}\mathbf{N}$, with $\mathbf{L}$ a differential operator:

$$\mathbf{L} = \begin{bmatrix} \frac{\partial}{\partial x} & 0 \\ 0 & \frac{\partial}{\partial y} \\ \frac{\partial}{\partial y} & \frac{\partial}{\partial x} \end{bmatrix}, \tag{9}$$

for two dimensions and $\mathbf{R}$ a matrix containing the components of the vector $\mathbf{n} = [n_x, n_y]^\mathrm{T}$ which is normal to the discontinuity, pointing into the Ω^+ domain,

$$\mathbf{R} = \begin{bmatrix} n_x & 0 \\ 0 & n_y \\ n_y & n_x \end{bmatrix}. \tag{10}$$

3.1 Variational formulation

Neglecting body forces, the weak equation for the static equilibrium is written as:

$$\int_{\Omega} \nabla^s \boldsymbol{\eta} : \boldsymbol{\sigma} \, \mathrm{d}\Omega = \int_{\Gamma_u} \boldsymbol{\eta} \cdot \bar{\mathbf{t}} \, \mathrm{d}\Gamma, \tag{11}$$

where $\boldsymbol{\eta}$ are admissible displacement variations, $\boldsymbol{\sigma}$ is the stress field and $\bar{\mathbf{t}}$ are the external tractions. The admissible displacement variations are taken the same as the displacement functions (see equation (1)):

$$\boldsymbol{\eta} = \hat{\boldsymbol{\eta}} + \mathscr{H}_{\Gamma_d} \tilde{\boldsymbol{\eta}} \, . \tag{12}$$

Inserting equation (12) into equation (11) yields:

$$\int_{\Omega} \nabla^s (\hat{\boldsymbol{\eta}} + \mathscr{H}_{\Gamma_d} \tilde{\boldsymbol{\eta}}) : \boldsymbol{\sigma} \, \mathrm{d}\Omega = \int_{\Gamma_u} (\hat{\boldsymbol{\eta}} + \mathscr{H}_{\Gamma_d} \tilde{\boldsymbol{\eta}}) \cdot \bar{\mathbf{t}} \, \mathrm{d}\Gamma, \tag{13}$$

and taking the gradient of $\boldsymbol{\eta}$,

$$\int_{\Omega} [(\nabla^s \hat{\boldsymbol{\eta}} + \mathscr{H}_{\Gamma_d} \nabla^s \tilde{\boldsymbol{\eta}}) : \boldsymbol{\sigma} + \delta_{\Gamma_d} (\tilde{\boldsymbol{\eta}} \otimes \mathbf{n})^s : \boldsymbol{\sigma}] \, \mathrm{d}\Omega = \int_{\Gamma_u} (\hat{\boldsymbol{\eta}} + \mathscr{H}_{\Gamma_d} \tilde{\boldsymbol{\eta}}) \cdot \bar{\mathbf{t}} \, \mathrm{d}\Gamma. \tag{14}$$

The Heaviside functions can be eliminated from the integrals by changing the integration domain from Ω to Ω^+. The term with the Dirac-delta function can be transformed into a surface integral over the discontinuity Γ_d by using the integral properties of the Dirac-delta function. Rearranging equation (14) gives:

$$\int_{\Omega} \nabla^s \hat{\boldsymbol{\eta}} : \boldsymbol{\sigma} \, \mathrm{d}\Omega + \int_{\Omega^+} \nabla^s \tilde{\boldsymbol{\eta}} : \boldsymbol{\sigma} \, \mathrm{d}\Omega + \int_{\Gamma_d} \tilde{\boldsymbol{\eta}} \cdot \mathbf{t} \, \mathrm{d}\Gamma = \int_{\Gamma_u} (\tilde{\boldsymbol{\eta}} + \mathscr{H}_{\Gamma_d} \tilde{\boldsymbol{\eta}}) \cdot \bar{\mathbf{t}} \, \mathrm{d}\Gamma, \tag{15}$$

where $\mathbf{t} = \boldsymbol{\sigma}\mathbf{n}$, the traction acting across the discontinuity. Taking the variations $\hat{\boldsymbol{\eta}}$ and $\tilde{\boldsymbol{\eta}}$, respectively, gives:

$$\int_{\Omega} \nabla \hat{\boldsymbol{\eta}} : \boldsymbol{\sigma} \, \mathrm{d}\Omega = \int_{\Gamma_u} \tilde{\boldsymbol{\eta}} \cdot \bar{\mathbf{t}} \, \mathrm{d}\Gamma, \tag{16a}$$

$$\int_{\Omega^+} \nabla \tilde{\boldsymbol{\eta}} : \boldsymbol{\sigma} \, \mathrm{d}\Omega + \int_{\Gamma_d} \tilde{\boldsymbol{\eta}} \cdot \mathbf{t} \, \mathrm{d}\Gamma = \int_{\Gamma_u} \mathscr{H}_{\Gamma_d} \tilde{\boldsymbol{\eta}} \cdot \bar{\mathbf{t}} \, \mathrm{d}\Gamma. \tag{16b}$$

3.2 Discretised, linearised equations

The discrete form of the weak equations (16a) and (16b) can be formed by inserting the discrete expressions for the displacement and test functions:

$$\begin{aligned} \hat{\mathbf{u}} &= \mathbf{N}\mathbf{a}; & \tilde{\mathbf{u}} &= \mathbf{N}\mathbf{b}; \\ \nabla\hat{\mathbf{u}} &= \mathbf{B}\mathbf{a}; & \nabla\tilde{\mathbf{u}} &= \mathbf{B}\mathbf{b}; \\ \hat{\boldsymbol{\eta}} &= \mathbf{N}\mathbf{a}'; & \tilde{\boldsymbol{\eta}} &= \mathbf{N}\mathbf{b}'; \\ \nabla\hat{\boldsymbol{\eta}} &= \mathbf{B}\mathbf{a}'; & \nabla\tilde{\boldsymbol{\eta}} &= \mathbf{B}\mathbf{b}', \end{aligned} \tag{17}$$

where the primes indicate the variations. The result is:

$$\int_{\Omega} \mathbf{B}^{\mathrm{T}} \boldsymbol{\sigma} \, \mathrm{d}\Omega = \int_{\Gamma_u} \mathbf{N}^{\mathrm{T}} \bar{\mathbf{t}} \, \mathrm{d}\Gamma, \tag{18a}$$

$$\int_{\Omega^+} \mathbf{B}^{\mathrm{T}} \boldsymbol{\sigma} \, \mathrm{d}\Omega + \int_{\Gamma_d} \mathbf{N}^{\mathrm{T}} \mathbf{t} \, \mathrm{d}\Gamma = \int_{\Gamma_u} \mathscr{H}_{\Gamma_\mathrm{d}} \mathbf{N}^{\mathrm{T}} \bar{\mathbf{t}} \, \mathrm{d}\Gamma. \tag{18b}$$

The stress rate in the bulk material is related to the strain rate via:

$$\dot{\boldsymbol{\sigma}} = \mathbf{D} \dot{\boldsymbol{\varepsilon}}, \tag{19}$$

where $\mathbf{D}$ is the tangential constitutive matrix. Using the bounded part of equation (2), which applies to the bulk, we obtain:

$$\dot{\boldsymbol{\sigma}} = \mathbf{D}\mathbf{B}(\dot{\mathbf{a}} + \mathscr{H}_{\Gamma_\mathrm{d}} \dot{\mathbf{b}}). \tag{20}$$

The traction rate at the discontinuity can be expressed in terms of the velocities of the additional degrees-of-freedom:

$$\dot{\mathbf{t}} = \mathbf{T}\mathbf{N}\dot{\mathbf{b}} \tag{21}$$

where $\mathbf{T}$ is the tangent matrix at the constitutive relation for the discontinuity. Inserting these relations into equations (18a) and (18b) gives:

$$\begin{bmatrix} \mathbf{K}_{aa} & \mathbf{K}_{ab} \\ \mathbf{K}_{ab} & \mathbf{K}_{bb} \end{bmatrix} \begin{bmatrix} \Delta\mathbf{a} \\ \Delta\mathbf{b} \end{bmatrix} = \begin{bmatrix} \mathbf{f}_a^{\mathrm{ext}} \\ \mathbf{f}_b^{\mathrm{ext}} \end{bmatrix} - \begin{bmatrix} \mathbf{f}_a^{\mathrm{int}} \\ \mathbf{f}_b^{\mathrm{int}} \end{bmatrix}, \tag{22}$$

for finite displacement increments, where the stiffness terms are:

$$\mathbf{K}_{aa} = \int_{\Omega} \mathbf{B}^{\mathrm{T}} \mathbf{D} \mathbf{B} \, \mathrm{d}\Omega; \qquad \mathbf{K}_{ab} = \int_{\Omega^+} \mathbf{B}^{\mathrm{T}} \mathbf{D} \mathbf{B} \, \mathrm{d}\Omega; \tag{23a}$$

$$\mathbf{K}_{bb} = \int_{\Omega^+} \mathbf{B}^{\mathrm{T}} \mathbf{D} \mathbf{B} \, \mathrm{d}\Omega + \int_{\Gamma_d} \mathbf{N}^{\mathrm{T}} \mathbf{T} \mathbf{N} \, \mathrm{d}\Gamma. \tag{23b}$$

The external force vectors are equal to:

$$\mathbf{f}_a^{\mathrm{ext}} = \int_{\Gamma_u} \mathbf{N}^{\mathrm{T}} \bar{\mathbf{t}} \, \mathrm{d}\Gamma; \qquad \mathbf{f}_b^{\mathrm{ext}} = \mathscr{H}_{\Gamma_\mathrm{d}} \int_{\Gamma_u} \mathbf{N}^{\mathrm{T}} \bar{\mathbf{t}} \, \mathrm{d}\Gamma. \tag{24}$$

The internal force vectors are equal to:

$$\mathbf{f}_a^{\mathrm{int}} = \int_{\Omega} \mathbf{B}^{\mathrm{T}} \boldsymbol{\sigma} \, \mathrm{d}\Omega; \qquad \mathbf{f}_b^{\mathrm{int}} = \int_{\Omega^+} \mathbf{B}^{\mathrm{T}} \boldsymbol{\sigma} \, \mathrm{d}\Omega + \int_{\Gamma_d} \mathbf{N}^{\mathrm{T}} \mathbf{t} \, \mathrm{d}\Gamma. \tag{25}$$

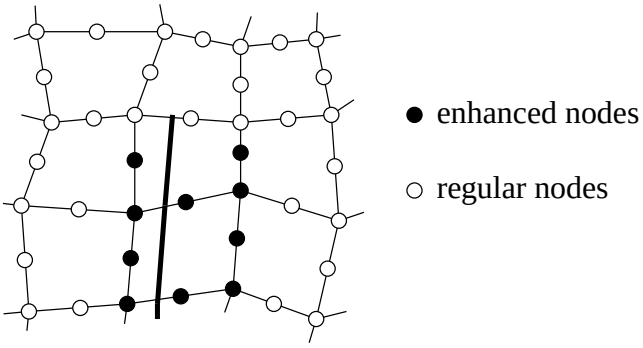

Figure 2: Group of eight-noded quadrilateral elements with a discontinuity (bold line). The enhanced nodes contain additional degrees of freedom.

4 Implementation

The procedure is implemented in four and eight-noded two-dimensional quadrilateral elements. It is assumed that a discontinuity within an element is a straight line, which implies that the normal vector **n** is constant within the element. The four and eight-noded elements are integrated numerically with a 4×4 and a 6×6 Gauss integration scheme, respectively, so that for nearly all positions of the discontinuity, both parts of the element (Ω^- and Ω^+) are covered with a sufficient amount of integration points. The integrals over the Γ_d domain, can be evaluated with different integration schemes (e.g. Gauss, Newton-Cotes) with a variable number of integration points. Elements which are not crossed by the discontinuity can be integrated with the standard integration schemes for quadrilateral elements. Hence, the extra computational effort is limited.

Moreover, the discontinuity is only introduced through the entire element. Consequently, a crack tip is always located at the edge of an element, as shown in Figure 2. This simplifies the model significantly, but leads to stress jumps, at the sudden introduction of the discontinuity. However, this has no influence on the robustness and stability of the numerical procedure [5]. The nodes on the boundary of the element touched by the crack tip do not have additional degrees of freedom, as can be seen in Figure 2. Doing so, the separation at the tip of the discontinuity is equal to zero.

The implementation of the enhanced elements with an elastic dummy stiffness for the discontinuity, the incorporated interface elements, is more straightforward. Since the trajectory of the crack is known beforehand, the surrounding nodes can be enhanced a priori.

5 Constitutive models

Delamination growth in laminates with different material properties per layer is a combination of mode-I and mode-II cracking. In previous studies with conventional interface elements, an orthotropic damage model was derived [8, 9, 10]. This model can be adapted to the current finite element descriptions in a straightforward manner. Presently, an ad-hoc mode-I delamination model has been implemented, used previously by Wells *et al.* [11]. In it, a loading function f is

defined as:

$$f(\tilde{u}_n, \kappa) = \tilde{u}_n - \kappa\,, \tag{26}$$

where $\tilde{u}_n$ is the normal separation of the crack and κ a history parameter. This history parameter is equal to the largest value of $\tilde{u}_n$ reached hitherto. When $f = 0$, loading occurs and when $f < 0$ there is unloading. The normal traction force t_n at the crack edges decreases exponentially, according to the following equation:

$$t_n = f_t \exp\Big(-\frac{f_t}{G_f}\kappa\Big)\,, \tag{27}$$

where f_t is the ultimate tensile strength and G_f the fracture toughness. The traction in the transverse direction t_s is equal to zero. In order to have quadratic convergence in a Newton-Raphson procedure for obtaining equilibrium at a structural level, a consistently linearised tangent matrix $\mathbf{T}$ has been derived:

$$\mathbf{T} = \begin{bmatrix} -\frac{f_t^2}{G_f}\exp\big(-\frac{f_t}{G_f}\kappa\big) & 0 \\ 0 & 0 \end{bmatrix}. \tag{28}$$

This tangent matrix does not have an elastic counterpart, since the tractions are only calculated when the discontinuity has been initiated.

In the incorporated interface element, the material model is slightly different. Prior to crack growth, the tractions depend on the separation of the crack via an elastic dummy stiffness D:

$$\begin{bmatrix} t_n \\ t_s \end{bmatrix} = \begin{bmatrix} D & 0 \\ 0 & 0 \end{bmatrix} \begin{bmatrix} u_n \\ u_s \end{bmatrix}. \tag{29}$$

Crack growth is initiated when the equivalent normal separation in the interface exceeds a threshold value $\kappa_0 \neq 0$. Therefore, the loading function is formulated as:

$$f(\tilde{u}_n, \kappa) = \tilde{u}_n - \kappa; \qquad \text{where} \quad \kappa = \max\Big[\kappa_{\text{prev}}, \kappa_0\Big]\,. \tag{30}$$

Consequently, the softening law is also different:

$$t_n = f_t \exp\left(-\frac{f_t}{G_f}\big(\kappa - \kappa_0\big)\right). \tag{31}$$

Quadratic convergence is obtained by applying a consistently linearised tangent matrix $\mathbf{T}$, which is similar to the total enhanced material model in equation (28).

6 Numerical examples

Examples are now presented to illustrate the accuracy of the proposed formulation. All calculations have been performed with conventional interface elements, with the incorporated interface elements and with the total enhanced elements.

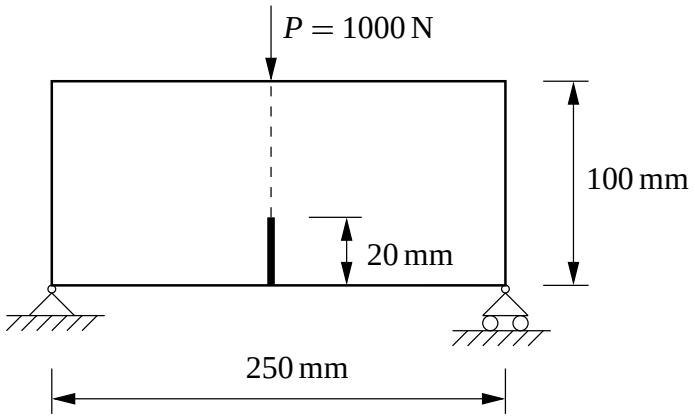

Figure 3: Geometry of a notched beam in a three point bending test.

6.1 Three point bending test

In the first example, the performance of the incorporated interface elements is examined by means of a three point bending test. Conventional interface elements suffer from spurious stress oscillations for high ratios of dummy stiffnesses and the Young's modulus of the continuum elements [2]. These oscillations can be eliminated by either reducing the dummy stiffness or by applying an alternative integration method.

Consider a beam as shown in Figure 3. The beam is supported on both sides and has a notch in the centre. The beam is made of an elastic, isotropic material with Young's modulus $E = 20\,000$ N/mm^2 and a Poisson's ratio $\nu = 0.2$. The model consists of 51×20 four-noded or 25×10 eight-noded elements. Both the notch and the interface in front of the notch are modelled with incorporated interface elements. The notch is simulated as a traction-free discontinuity, the remaining incorporated interface elements are equipped with a linear elastic material model. Calculations have been carried out for different values of the dummy stiffness D and for different integration schemes. The traction profiles, as a function of the distance from the notch, are shown in Figures 4 to 6 for different cases.

The incorporated interface elements show the same stress oscillations as the standard interface elements. The elements produce correct results if the dummy stiffness is not too high in comparison with the stiffness of the continuum. When the dummy stiffness increases, a Gauss integration scheme exhibits stress oscillations. A Newton-Cotes integration scheme gives correct results for all ranges of the dummy stiffness. Nevertheless, in Figure 6 it is shown that over-integration with this scheme again results in stress oscillations. Therefore, in the remainder, we will integrate the discontinuity terms in the four-noded incorporated interface elements with a two point Newton-Cotes integration scheme and in the eight-noded elements with a three point Newton-Cotes scheme. The discontinuity of the total enhanced elements will still be integrated with a Gauss integration scheme.

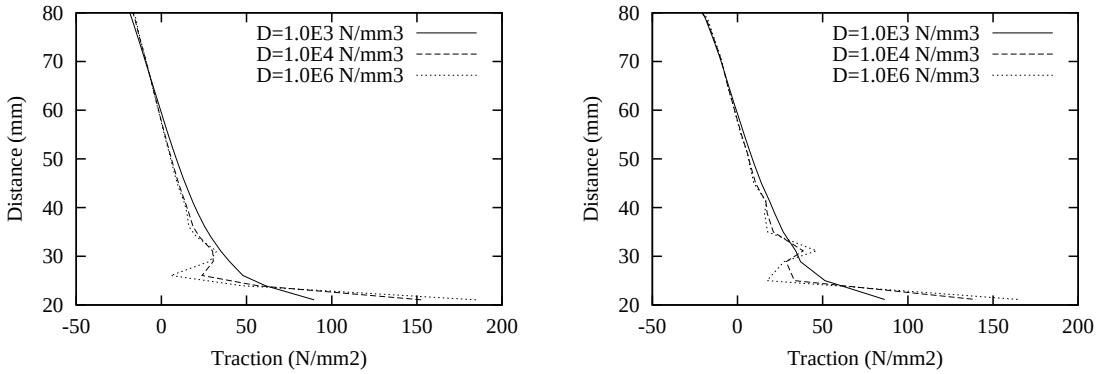

(a) Linear elements (b) Quadratic elements

Figure 4: Traction profiles at the interface of the notched beam (Gauss integration scheme).

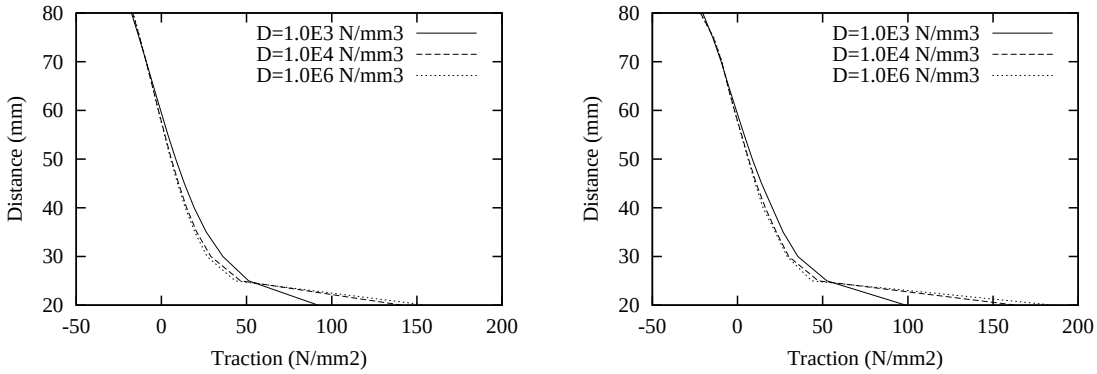

(a) Linear elements (b) Quadratic elements

Figure 5: Traction profiles at the interface of notched beam (Newton-Cotes integration scheme).

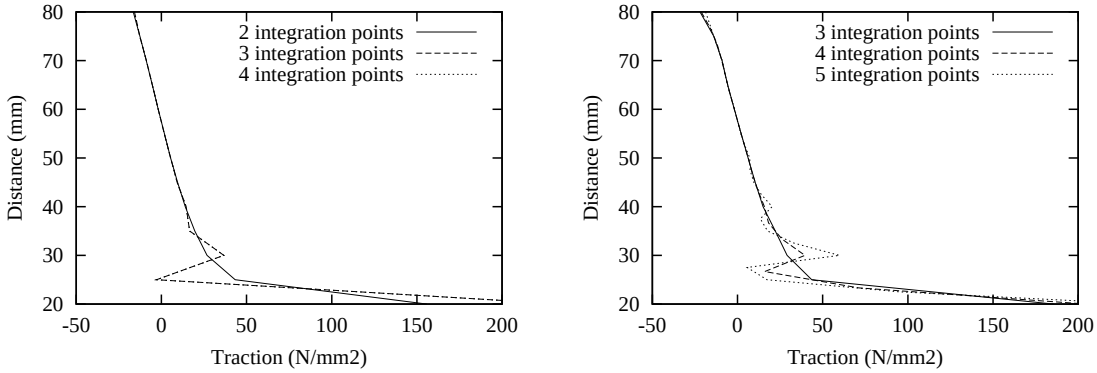

(a) Linear elements (b) Quadratic elements

Figure 6: Effects of over-integration on the traction profiles of the interface of the notched beam with a Newton-Cotes integration scheme.

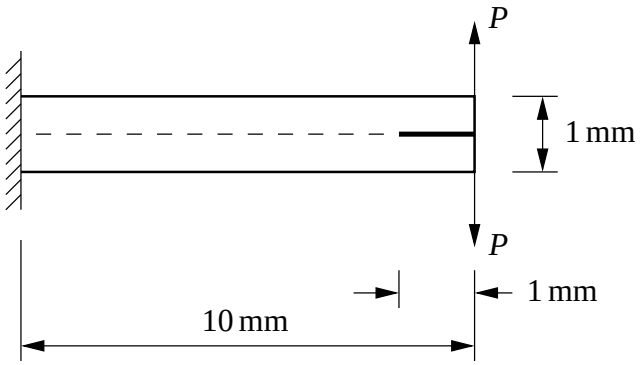

Figure 7: Geometry of clamped laminate subjected to a peel test.

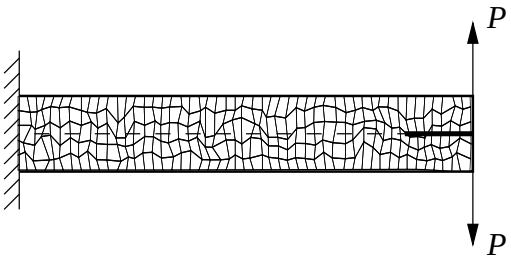

Figure 8: Finite element model with unstructured mesh (eight-noded elements)

6.2 A peel test

We now consider the laminate shown in Figure 7. The laminate consists of two layers with the same thickness and with identical isotropic material properties, $E = 100\,\mathrm{N/mm^2}$ and $\nu = 0.3$. The two layers are connected with an adhesive. The ultimate tensile strength of this material equals $f_t = 1\,\mathrm{N/mm^2}$, the fracture toughness is $G_f = 0.1\,\mathrm{N/mm}$. Since the stress state at the interface is expected to be purely in mode-I, the shear stiffness equals zero. The first millimetre is assumed to be debonded. An external load P is applied at the tips of both layers.

The specimen has been analysed with both numerical approaches: the incorporated interface elements and the total enhanced elements. These element have been used in structured and unstructured meshes (see Figure 8). The model contains 70×7 four-noded or 50×5 eight-noded elements. Conventional interface elements have been used also. The dummy stiffness in these elements and in the incorporated interface elements is set to $D = 10^6\,\mathrm{N/mm^3}$.

The results of the analysis with the various models are given in the Figures 9 - 11. All methods give nearly identical results for both structured and unstructured meshes.

7 Conclusions

The application of enhanced elements in the simulation of delamination growth has been discussed. The enhancement has been applied in two ways, as an incorporated interface element

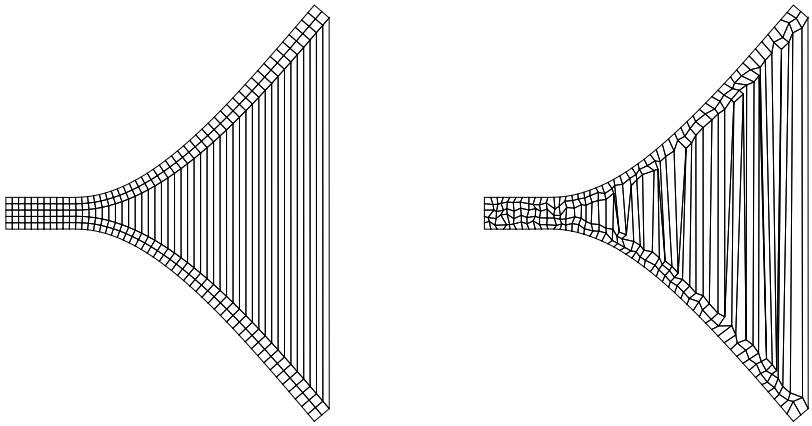

Figure 9: Deformation plot for peel test with a structured mesh (left) and an unstructured mesh.

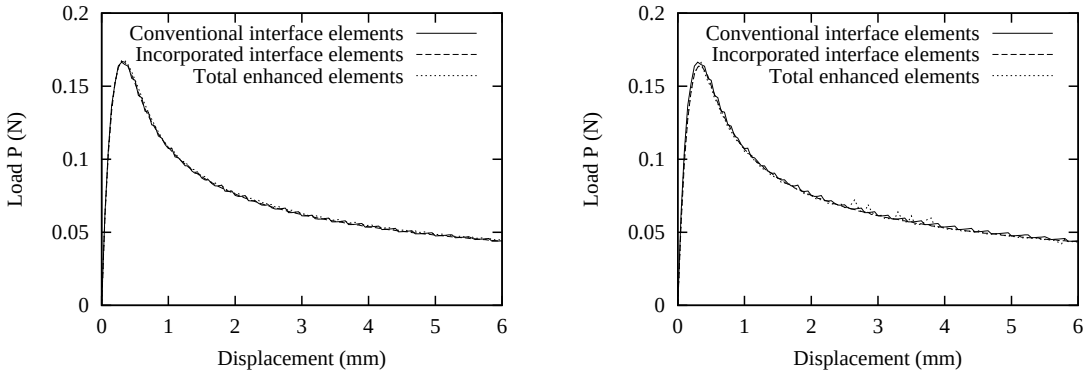

(a) Linear elements (b) Quadratic element

Figure 10: Load vs. displacement for different element types for structured meshes.

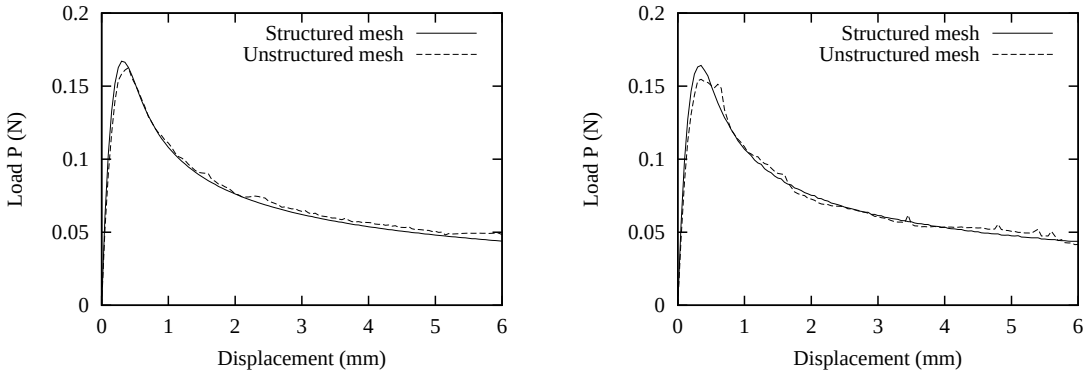

(a) Linear elements (b) Quadratic elements

Figure 11: Load vs. displacement for structured and unstructured meshes with incorporated interface elements.

with a dummy interface stiffness prior to cracking and as an total enhanced continuum element. Debonding has been modelled with a mode-I traction-separation law. The results of the analyses of two simple structures have been compared for both formulations and with conventional interface elements.

The incorporated interface element with a dummy stiffness exhibits the same stress oscillations prior to cracking as was observed with the interface elements. Alternative integration schemes and/or a reduced dummy stiffness are a solution to this inconveniency [1, 2]. Both this element and the total enhanced elements have shown to be robust and numerically stable in a peel test. Good results have been obtained even for unstructured meshes.

The method is appealing both from a theoretical and computational point of view. It is mathematically more consistent than conventional interface models. The simulation of more complicated failure mechanisms is possible as well, since the crack path is independent from the finite element mesh.

Acknowledgement

Financial support for the second author from the Netherlands Technology Foundation (STW) is gratefully acknowledged.

References

[1] J.C.J. Schellekens. *Computational Strategies for Composite Structures*. PhD thesis, Delft University of Technology, Delft, The Netherlands, (1992).

[2] J.C.J. Schellekens and R. de Borst. On the numerical integration of interface elements. *Int. J. Num. Meth. Engng.*, **36**, 43–66, (1993).

[3] I. Babuška and J.M. Melenk. The partition of unity method. *Int. J. Num. Meth. Engng.*, **40 (4)**, 727–758, (1997).

[4] C.A. Duarte and J.T. Oden. H-p clouds – an h-p meshless method. *Numerical Methods for Partial Differential Equations*, **12 (6)**, 673–705, (1996).

[5] G.N. Wells and L.J. Sluys. A new method for modelling cohesive cracks using finite elements. *Int. J. Num. Meth. Engng.*, **50**, 2667–2682, (2001).

[6] G.N. Wells and L.J. Sluys. Discontinuous analysis of softening solids under impact loading. *Int. J. Numer. Anal. Meth. Geomech.*, **25 (7)**, (2001).

[7] O.C. Zienkiewicz and R.L. Taylor. *The Finite Element Method, Vol. 1, Basic Formulation and Linear Problems*. Mc-Graw Hill, (1989).

[8] J. Lemaitre and J.L. Chaboche. *Mechanics of Solid Materials*. Cambridge University Press, (1990).

[9] O. Allix and P. Ladevèze. Modelling and computation of delamination for composite laminates. *Arch. Mech.*, **44**, 5–13, (1992).

[10] J.J.C. Remmers and R. de Borst. Delamination buckling in fibre-metal laminates. *Composite Science and Technology*, accepted.

[11] G.N. Wells and L.J. Sluys. Three-dimensional embedded discontinuity model for brittle fracture. *International Journal of Solids and Structures*, **38 (5)**, 897–913, (2001).